Article

Modification of CeNi$_{0.9}$Zr$_{0.1}$O$_3$ Perovskite Catalyst by Partially Substituting Yttrium with Zirconia in Dry Reforming of Methane

Mahmud S. Lanre [1], Ahmed E. Abasaeed [1,*], Anis H. Fakeeha [1], Ahmed A. Ibrahim [1,*], Abdullah A. Alquraini [1], Salwa B. AlReshaidan [2] and Ahmed S. Al-Fatesh [1,*]

[1] Chemical Engineering Department, College of Engineering, King Saud University, P.O. Box 800, Riyadh 11421, Saudi Arabia; mahmudsofiu@gmail.com (M.S.L.); anishf@ksu.edu.sa (A.H.F.); abalquraini@ksu.edu.sa (A.A.A.)

[2] Department of Chemistry, College of Science, King Saud University, Riyadh 11451, Saudi Arabia; chem@ksu.edu.sa

* Correspondence: abasaeed@ksu.edu.sa (A.E.A.); aididwthts2011@gmail.com (A.A.I.); aalfatesh@ksu.edu.sa (A.S.A.-F.); Tel.: +966-11-467-6856 (A.E.A. & A.A.I.); +966-11-467-6859 (A.S.A.-F.)

Abstract: Methane Dry Reforming is one of the means of producing syngas. CeNi$_{0.9}$Zr$_{0.1}$O$_3$ catalyst and its modification with yttrium were investigated for CO$_2$ reforming of methane. The experiment was performed at 800 °C to examine the effect of yttrium loading on catalyst activity, stability, and H$_2$/CO ratio. The catalyst activity increased with an increase in yttrium loading with CeNi$_{0.9}$Zr$_{0.01}$Y$_{0.09}$O$_3$ catalyst demonstrating the best activity with CH$_4$ conversion >85% and CO$_2$ conversion >90% while the stability increased with increases in zirconium loading. The specific surface area of samples ranged from 1–9 m^2/g with a pore size of 12–29 nm. The samples all showed type IV isotherms. The XRD peaks confirmed the formation of a monoclinic phase of zirconium and the well-crystallized structure of the perovskite catalyst. The Temperature Program Reduction analysis (TPR) showed a peak at low-temperature region for the yttrium doped catalyst while the un-modified perovskite catalyst (CeNi$_{0.9}$Zr$_{0.1}$O$_3$) showed a slight shift to a moderate temperature region in the TPR profile. The Thermogravimetric analysis (TGA) curve showed a weight loss step in the range of 500–700 °C, with CeNi$_{0.9}$Zr$_{0.1}$O$_3$ having the least carbon with a weight loss of 20%.

Keywords: catalyst stability; dry reforming of methane; perovskite catalyst; catalyst activity

1. Introduction

Fossil fuels such as natural gas, coal, and crude oil serve as the backbone for the 21st century energy, industrial, and transportation sectors of the economy [1]. Their usage liberates CO$_2$ that accumulates over time in the atmosphere depleting the ozone layer shield of the earth, leading to the rising temperature of the earth causing global warming. The impact of this global warming on the environment includes ecosystem collapse, desertification, etc., and can have direct effects on humans such as extremely hot weather conditions, or indirect effects such as crop failure and farmland loss causing a food shortage. In order to save the earth, the emissions of the greenhouse gases must be drastically reduced; hence, this necessitates dry reforming of methane (DRM) reaction which employs methane and carbon dioxide greenhouse gases to produce syngas (H$_2$/CO), thereby controlling the mitigation of these two global warming gases [2]. DRM can also utilize biogas, composed mainly of CO$_2$ and CH$_4$. This reaction is strongly endothermic.

The dry reforming reaction comprises:

$$\text{Methane Dry Reforming: } CO_2 + CH_4 \leftrightarrow 2CO + 2H_2 \tag{1}$$

$$\text{Reverse Water-Gas Shift Reaction: } CO_2 + H_2 \leftrightarrow CO + H_2O \tag{2}$$

$$\text{Methane Cracking Reaction: } CH_4 \leftrightarrow C + H_2 \tag{3}$$

$$\text{Disproportionation Reaction: } 2CO \leftrightarrow C + CO_2 \tag{4}$$

$$\text{Carbon Gasification: } C + H_2O \leftrightarrow CO + H_2 \tag{5}$$
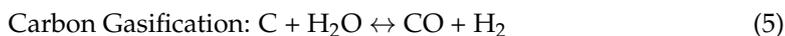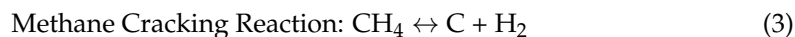
Synthesis gas (syngas) obtained from DRM reaction can be converted to methanol and synthetic fuels by Shell middle distillate synthesis (SMDS) or Fischer–Tropsch syntheses [3]. Hydrogen production is being increased during the conversion of CO with steam in water gas shift reaction to CO_2 [1]. Suitable catalysts for the DRM have been investigated using transition elements like Ni, Co, Pd, Ir, and perovskite-type oxides, which are very active [4]. Nickel catalysts are majorly considered for dry reforming reactions [5–8] based on its low price. However, coking and sintering cause the catalyst to deactivate [9,10]. The two major characteristics of the catalyst that defines coking are surface properties and acidity [11]. Carbon deposition depends on factors such as the nature of the hydrocarbon and the catalyst and reaction operating conditions [11]. Coking can be mitigated by supporting the active metal on a metal oxide with strong basicity [11]. Methane adsorption on nickel requires the bond breaking of C-H. The CH_4 is converted thus: $CH_4 \rightarrow CH_3^* \rightarrow CH_2^* \rightarrow CH^* \rightarrow C^*$ [11]. Ni catalysts are being bolstered so as to hamper carbon deposits and achieve good stability leading to the development of catalysts with an abundance of oxygen for coke gasification such as perovskite catalyst [12].

The structural stability of perovskite is altered by incorporating an atom into its structure resulting in changes in oxygen mobility [13]. It was reported that lower valent cations addition into perovskite catalyst structure resulted in oxygen ions adsorption onto the surfaces and changes to lattice oxygen. Such changes to the surface lattice oxygen ions would lead to various types of adsorption onto the surface of the perovskite catalyst structure and different mass transfer rates of oxygen [14]. Investigating the influence of cerium on nickel-based catalysts for hydrogen production and reported that the addition of the right amount of cerium can increase oxygen vacancies formation, which can activate oxygen-containing compounds to react with carbon species as soon as it forms [15]. Basically, zirconia is known to be a better support for active metal, due to heat stability and explicit characteristics such as acid-base and reduction-oxidation properties [16–20]. It has been proven that ZrO_2 is a proper support for Ni, as it gives restricted coke formation with a small carbon combustion temperature [21]. Yttrium oxide (Y_2O_3) can either be acting as a promoter or support as a result of its unique chemical and thermal properties. Y_2O_3 supported Ni catalyst allows the ease reduction, better activity, stability, and limits the reverse of water gas shift (RWGS) reaction [22]. Yttria-zirconia as support for DRM suggests that the supported Ni catalysts will gain from redox properties of the material which is exceptional to limit the carbonaceous deposit formation thereby increasing the lifetime of the catalyst [23–25]. Promoters like alkali earth and alkali with rare earth metals have been used for the activity and stability enhancement of nickel-based catalysts [26–28]. Doping of trace amounts of noble metals to Ni catalyst leads to direct improvements of the catalytic reaction features of DRM [29–31].

The aim of this work is to study the effect of $CeNi_{0.9}Zr_{0.1}O_3$ perovskite catalyst modified with yttrium on DRM. The incorporation of yttrium into the perovskite structure is evaluated in terms of catalyst activity, stability, amount, and nature of carbon formed.

2. Materials and Methods

The perovskite catalysts $CeNi_{0.9}Zr_{0.1-x}Y_xO_3$ (x = 0, 0.03, 0.05, 0.07, and 0.09) were prepared by the sol-gel method with propionic acid acting as a solvent, to dissolve nitrates of each metal. In the preparation, Ni $(NO_3)_2 \cdot 6H_2O$ (Sigma, St. Louis, MO, USA), Y$(NO_3)_3 \cdot 6H_2O$ (Sigma), Ce $(NO_3)_3 \cdot 6H_2O$ (Sigma), Zr $(NO_3)_4 \cdot 6H_2O$ (Sigma), and propionic acid ($C_3H_6O_2$, Sigma) were used. The nitrates were separately dissolved in propionic acid, stirred, and heated at T = 90 °C with oil as a heating medium. Afterward, the solutions were continuously stirred for about 2 h at T = 130 °C. Thereafter, the propionic acid was evaporated with a rotary evaporator at T = 70–80 °C until a gel was formed. The gel

obtained was dried at T = 90 °C overnight, and calcined at 725 °C for 4 h. The catalysts formed after calcination were ground into powder and used for the DRM reaction.

2.1. Catalytic Testing

The catalysts were tested for DRM at 800 °C reaction temperature under atmospheric pressure. A packed bed reactor stainless steel reactor (0.0091 m internal diameter; 0.3 m height) was used to perform the experiment. An amount of 0.10 g of catalyst was placed in the reactor on top of glass wool. Stainless steel, sheathed thermocouple K-type, axially positioned close to the catalyst bed was used to determine the temperature during the reaction. Preceding the reaction, activation of the perovskite catalysts was done at 700 °C with H_2. This lasted for 60 min and the remnant H_2 was purged with N_2. During the dry reforming reaction, the feed volume ratio was kept at 3:3:1 for CH_4, CO_2, and N_2 gases, respectively, with a space velocity of 42 L/h./g_{cat}. The outlet gas from the reactor was connected to an online Gas Chromatography (GC) with a thermal conductivity detector to analyze its composition. The CH_4, CO_2 conversion, and H_2/CO (syngas ratio) were calculated using Equations (4)–(6):

$$\text{Methane conversion } (\%) = \frac{CH_{4,in} - CH_{4,out}}{CH_{4,in}} * 100 \qquad (6)$$

$$\text{Carbon dioxide conversion } = \frac{CO_{2,in} - CO_{2,out}}{CO_{2,in}} * 100 \qquad (7)$$

$$\text{Syngas Ratio} = \frac{\text{mole of } H_2 \text{ produced}}{\text{mole of CO produced}} \qquad (8)$$

2.2. Catalyst Physicochemical Properties Determination

2.2.1. Nitrogen Physisorption

The perovskite catalysts surface area, as well the pore size distribution, was measured by N_2 adsorption–desorption at −196 °C using a Micromeritics Tristar II 3020 for porosity and surface area analyzer.

2.2.2. Hydrogen Temperature Programmed Reduction Analysis

A total of 70 mg of the sample was loaded inside the TPR sample holder of a Micromeritics apparatus. Thereafter, TPR measurements were performed at 150 °C using Ar gas for 30 min and then cooled to ambient temperature. Thereafter, the sample was heated in a furnace up to 800 °C ramping at 10 °C min^{-1}, in the atmosphere of H_2/Ar mixture (1:9 vol. %) at 40 mL/min. The thermal conductivity detector recorded H_2 consumption during the operation.

2.2.3. Thermo-Gravimetric (TGA) Analysis

Quantification of carbon deposits on the used catalysts was determined by TGA analysis. 10–15 mg of the used catalysts was filled in a platinum pan. Heating was performed at ambient temperature up to 1000 °C at 20 °C min^{-1} temperature ramp. Loss in mass was constantly monitored as the heating progressed.

2.2.4. X-ray Diffraction (XRD) Analysis

The X-ray Diffraction patterns of the perovskite catalysts were recorded on a Miniflex Rigaku diffractometer that was equipped with Cu Kα X-ray radiation. The device was run at 40 mA and 40 kV.

2.2.5. Transmission Electron Microscopy (TEM)

Transmission electron microscopy (JEOL JEM-2100F) with high resolution to give larger magnification was used to carry out the TEM measurement of both the fresh and used catalyst. The electron microscope operated at 200 kV produces the active metal nickel

particle sizes and depicts the morphology of carbon deposit on the used catalyst. Before the TEM measurement, the catalysts were first dispersed ultrasonically in ethanol at room temperature. Thereafter, the drop from the suspension was placed in a lacey carbon-coated Copper grid to produce the images.

2.2.6. Laser Raman (NMR-4500) Spectrometer

Laser Raman (NMR-4500) Spectrometer (JASCO, Tokyo, Japan) was used to record Raman spectra of the spent catalyst samples. The wavelength of the excitation beam was set to 532 nm, and an objective lens of $100\times$ magnification was used for the measurement. The laser intensity was adjusted to 1.6 mW. Each spectrum was received by averaging 3 exposures on 10 s. Spectra were recorded in the range 1200–3000 cm^{-1} (Raman shift) and were processed by using Spectra Manager Ver.2 software (JASCO, Tokyo, Japan).

3. Results

3.1. BET (Brunauer–Emmett–Teller) Analysis

The surface area of the catalysts does not vary largely with one another with pore volume less than one. The isotherm curves as shown in Figure 1 suggest that the materials are mesoporous in nature with pore diameter less than 50 nm. The isotherm linear plot of all the samples represents Type IV isotherm. This occurs due to capillary condensation of gases in the tiny pores of solid at pressures below the gas saturation pressure. The textural properties of the fresh catalyst are provided in Table 1.
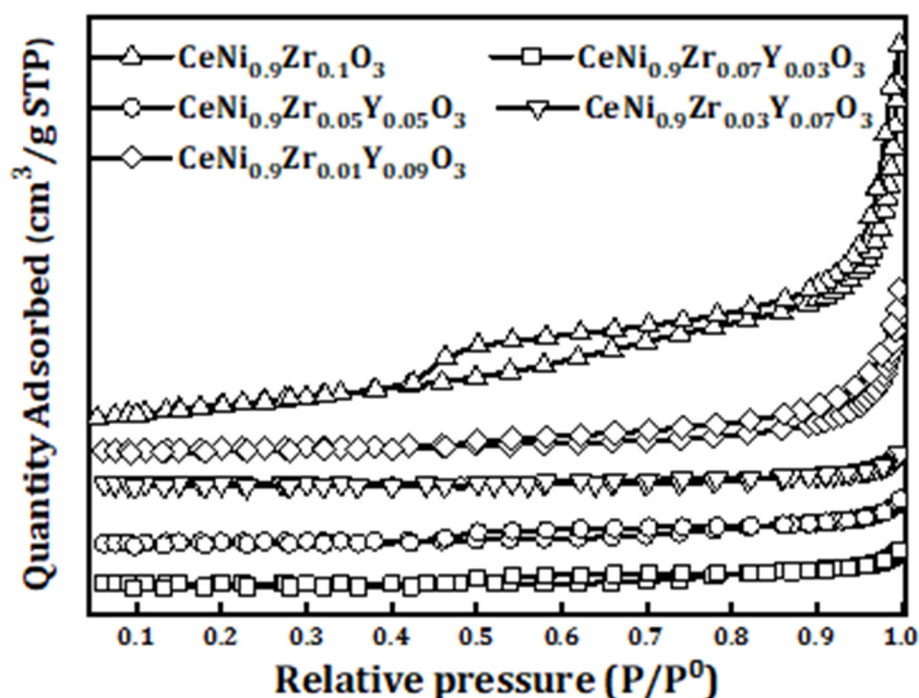

Figure 1. Nitrogen physisorption isotherms of perovskite catalyst $CeNi_{0.9}Zr_{0.1-x}Y_xO_3$ ($x = 0$, 0.03, 0.05, 0.07, and 0.09).

3.2. Temperature-Programmed Reduction (TPR)

The active sites for the catalyst samples are Ni and Zr, the samples are activated by H_2 reduction precedent to reaction. The reducibility of the catalyst samples was performed as shown in Figure 2. Peaks at the lower region are almost the same but there is a shoulder peak for un-modified sample in the moderate temperature region in the TPR profile. It has been reported that the reduction becomes easier while the energy of the metal–oxygen bond decreases [32]. The peaks at moderate temperature regions can be attributed to the reduction of Ni^{3+} to Ni^{2+}.

Table 1. Tabular presentation of Specific surface area (SSA), Pore volume (P_v), and Pore diameter (P_d) of the fresh catalyst samples.

Samples	SSA (m^2/g)	P_v (cm^3/g)	P_d (nm)
$CeNi_{0.9}Zr_{0.1}O_3$	9.35	0.031	12.12
$CeNi_{0.9}Zr_{0.07}Y_{0.03}O_3$	1.27	0.003	15.44
$CeNi_{0.9}Zr_{0.05}Y_{0.05}O_3$	1.62	0.003	14.43
$CeNi_{0.9}Zr_{0.03}Y_{0.07}O_3$	1.85	0.002	22.21
$CeNi_{0.9}Zr_{0.01}Y_{0.09}O_3$	2.66	0.011	29.33
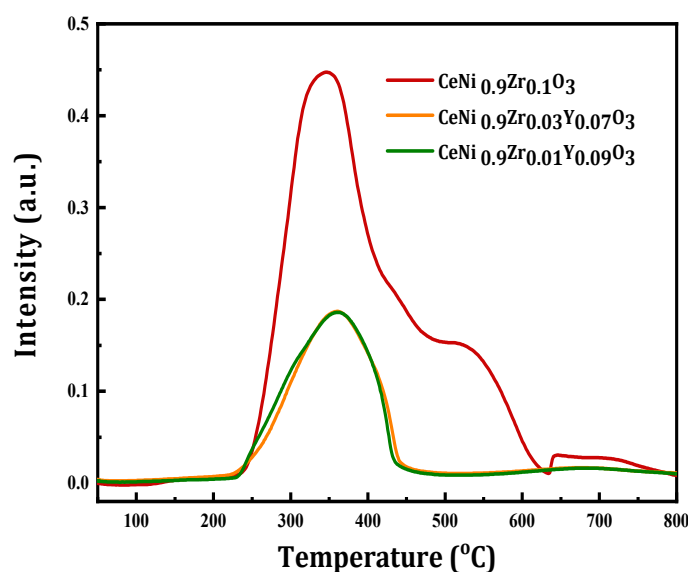
Figure 2. H_2-TPR profiles of perovskite catalyst $CeNi_{0.9}Zr_{0.1-x}Y_xO_3$ (x = 0, 0.07 and 0.09).

3.3. X-ray Diffraction (XRD) Analysis

The XRD peaks of the perovskite catalysts are depicted in Figures 3 and 4. At Y = 0.03–0.05, no XRD peaks of ZrO_2 phases are observed. In other samples, cubic zirconia oxide (JCPDS card reference number 00-020-0684) or tetragonal zirconium oxide (JCPDS card reference number 01-081-1547) or both phases are found. The XRD peaks confirm the formation of tetragonal and cubic zirconia [33,34]. The peaks from the XRD include cubic CeO_2 (JCPDS card reference number 01-002-1306), cubic NiO (JCPDS card reference number 00-002-1216), and cubic yttrium cerium oxide (JCPDS card reference number 01-075-0177). For the $CeNi_{0.9}Zr_{0.1}O_3$ catalyst, the intensity of the peaks at $2\theta = 28.5°$ and $48.2°$ are higher, suggesting a discrete crystalline phase of CeO_2 formation. The Ni in the Ce-Ni systems exists as NiO on the ceria surface and Ni^{2+} ions in the CeO_2 lattice [35,36]. The catalyst $CeNi_{0.9}Zr_{0.03}Y_{0.07}O_3$ had an additional rhombohedral nickel yttrium phase (JCPDS card reference number 00-020-0646).

3.4. Transmission Electron Microscope (TEM) Analysis

The TEM analysis for both the fresh and spent catalysts are illustrated in Figures 5 and 6 at 200 nm magnification. The used $CeNi_{0.9}Zr_{0.01}Y_{0.09}O_3$ catalyst particles are shown with the carbon spreading across the surface. The nickel particle size distribution expressed in the nanometer is plotted for each of the TEM images with that of the spent catalyst higher than the fresh catalyst samples and the result tabulated in Table 2.
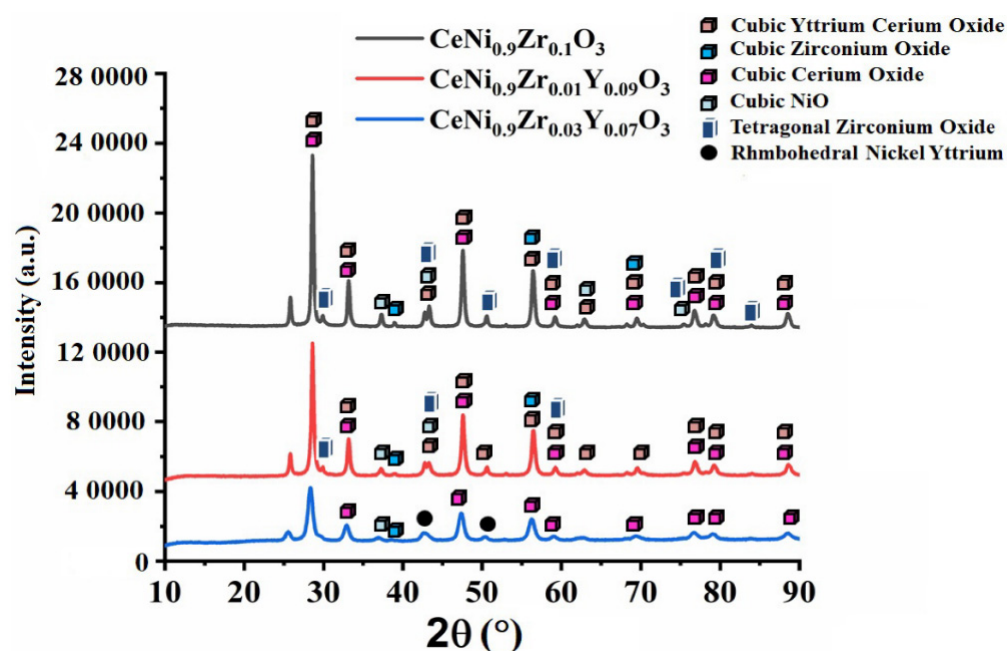
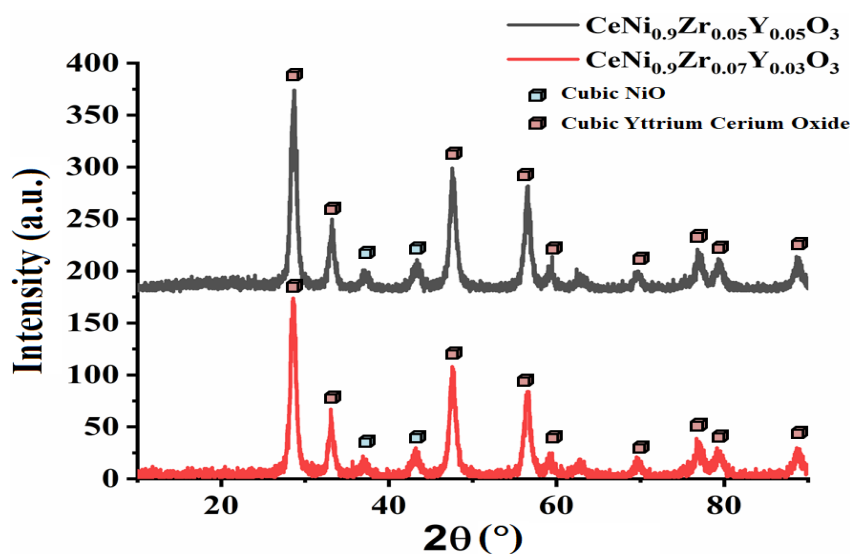**Figure 3.** XRD pattern of perovskite catalyst $CeNi_{0.9}Zr_{0.1-x}Y_xO_3$ (x = 0.00, 0.07 and 0.09).

Figure 4. XRD pattern of perovskite catalyst $CeNi_{0.9}Zr_{0.1-x}Y_xO_3$ (x = 0.03 and 0.05).

Table 2. Summary of Nickel Particle Size Derived from TEM Analysis.

Name	Ni Particle Size
Fresh $CeNi_{0.9}Zr_{0.1}O_3$	9.44 nm
Used $CeNi_{0.9}Zr_{0.1}O_3$	11.68 nm
Fresh $CeNi_{0.9}Zr_{0.01}Y_{0.09}O_3$	6.66 nm
Used $CeNi_{0.9}Zr_{0.01}Y_{0.09}O_3$	7.10 nm

3.5. Catalyst Activity

A varying amount of yttrium was used to modify the catalyst $CeNi_{0.9}Zr_{0.1-x}Y_xO_3$ with x = 0, 0.03, 0.05, 0.07, and 0.09) and tested at 800 °C for DRM reaction. The activity of the yttrium modified catalyst $CeNi_{0.9}Zr_{0.07}Y_{0.03}O_3$ was lower than the un-modified catalyst $CeNi_{0.9}Zr_{0.1}O_3$ and had the lowest activity for all the tested catalysts. The activity of the $CeNi_{0.9}Zr_{0.05}Y_{0.05}O_3$ catalyst is slightly higher than the un-modified $CeNi_{0.9}Zr_{0.1}O_3$ catalyst,

with the latter having 87% CO_2 and 78% CH_4 conversion, as shown in Figures 7 and 8. The activity of yttrium modified catalyst $CeNi_{0.9}Zr_{0.1-x}Y_xO_3$ when $x = 0.07$ and 0.09 is higher than the un-modified $CeNi_{0.9}Zr_{0.1}O_3$ catalyst. The former has 87% CH_4 and 90% CO_2 for $x = 0.07$, and 90% CH_4 and 91% CO_2 for $x = 0.09$. Yttrium results in oxygen vacancies formations that are believed to contribute to improved catalytic activity [37,38]. The catalyst activity increases with Y loading increase. Figure 9 displays the syngas ratios. The H_2/CO ratio values for $CeNi_{0.9}Zr_{0.1}O_3$ and $CeNi_{0.9}Zr_{0.07}Y_{0.03}O_3$ catalyst are less than one which suggests that the predominant side reaction is RWGS while $CeNi_{0.9}Zr_{0.05}Y_{0.05}O_3$, $CeNi_{0.9}Zr_{0.03}Y_{0.07}O_3$, $CeNi_{0.9}Zr_{0.01}Y_{0.09}O_3$ catalyst have H_2/CO ratio greater than one which suggests that the Boudouard reaction is the predominant side reaction. CeO_2 impregnated with yttrium increases ionic conductivity with Ce and Y bonded together, suggesting the possible presence of the CeO_2-Y_2O_3 phase, which favors NiO dispersion and limits the sintering [28]. Y_2O_3 as a basic carrier allows Ni catalyst to be easily reduced and have a better activity [29]. Yttrium enhances smaller nickel crystallites, thereby improving the dispersion of active sites. The promotion with 0.09Y led to better activity which was linked to the formation of a solid solution of ZrO_2-Y_2O_3, thereby enhancing the reduction of bulk NiO [29]. In addition, a number of oxygen vacancies and mobility can be enhanced by doping cerium with yttrium [39]. Ions of Ce^{3+} (0.97 Å) can be substituted by Y^{3+} (1.04 Å) and form a solid solution due to their similar ionic radii [39].
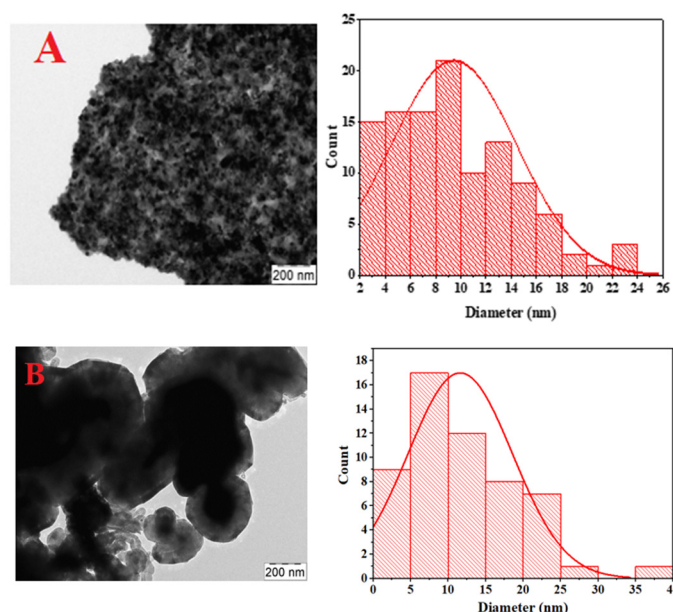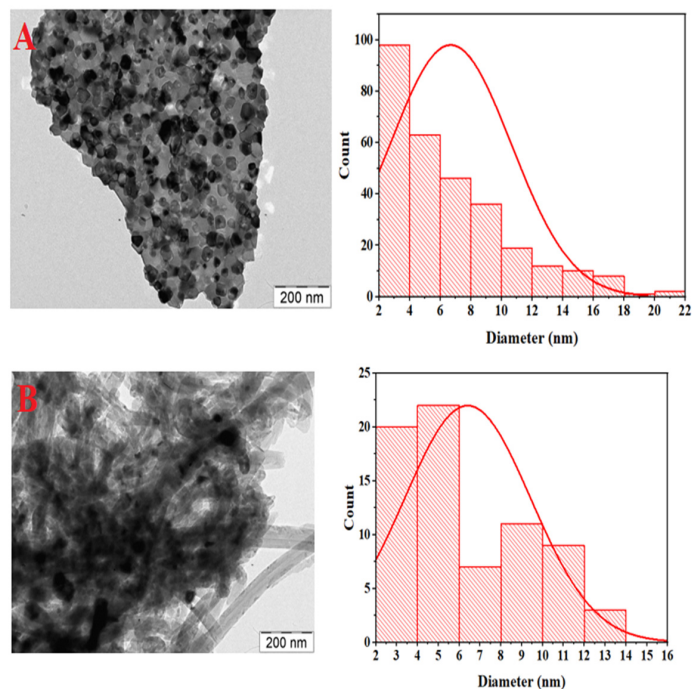

Figure 5. TEM micrographs and matching particle size distribution for fresh $CeNi_{0.9}Zr_{0.1}O_3$ (**A**) and used $CeNi_{0.9}Zr_{0.1}O_3$ (**B**) catalyst.

3.6. Thermogravimetric Analysis of the Used Catalyst (TGA)

The TGA curve of the spent catalysts was plotted in Figure 10 showing the weight loss of each catalyst expressed in percentage. The weight loss of the spent catalyst is shown to be 20%, 30%, 40%, 50%, and 55% for $CeNi_{0.9}Zr_{0.1}O_3$, $CeNi_{0.9}Zr_{0.07}Y_{0.03}O_3$, $CeNi_{0.9}Zr_{0.05}Y_{0.05}O_3$, $CeNi_{0.9}Zr_{0.03}Y_{0.07}O_3$, and $CeNi_{0.9}Zr_{0.01}Y_{0.09}O_3$, respectively. The $CeNi_{0.9}Zr_{0.1}O_3$ catalyst has the lowest amount of carbon compared to modified yttrium catalysts due to the former having a lesser amount of zirconium. The amount of carbon deposited on the catalyst increases with decreases in zirconium amount.

3.7. RAMAN Analysis

Raman spectra of the used catalysts (Figure 11) depict two bands with Raman shifts in the range of 1574 ± 5 cm^{-1} and 2650 ± 10 cm^{-1}, corresponding to the D and G bands respectively. The D band is related to coke deposits with imperfect, that is, disordered

structure (amorphous carbon), while the G band is related to well-ordered structure (graphitic carbon). The I_D/I_G ratio is less than one since I_D is less than I_G for used catalyst $CeNi_{0.9}Zr_{0.1-x}Y_xO_3$ when $x = 0$, 0.03 and 0.05; hence, it contains imperfect (amorphous carbon) on the catalyst surface after reaction while on the other hand for $CeNi_{0.9}Zr_{0.1-x}Y_xO_3$ catalysts where $x = 0.07$ and 0.09 have more graphitic carbon as the I_D/I_G ratio is greater than one for these catalysts.

Figure 6. TEM micrographs and matching particle size distribution for fresh $CeNi_{0.9}Zr_{0.01}Y_{0.09}O_3$. (**A**) and used $CeNi_{0.9}Zr_{0.01}Y_{0.09}O_3$. (**B**) catalyst.
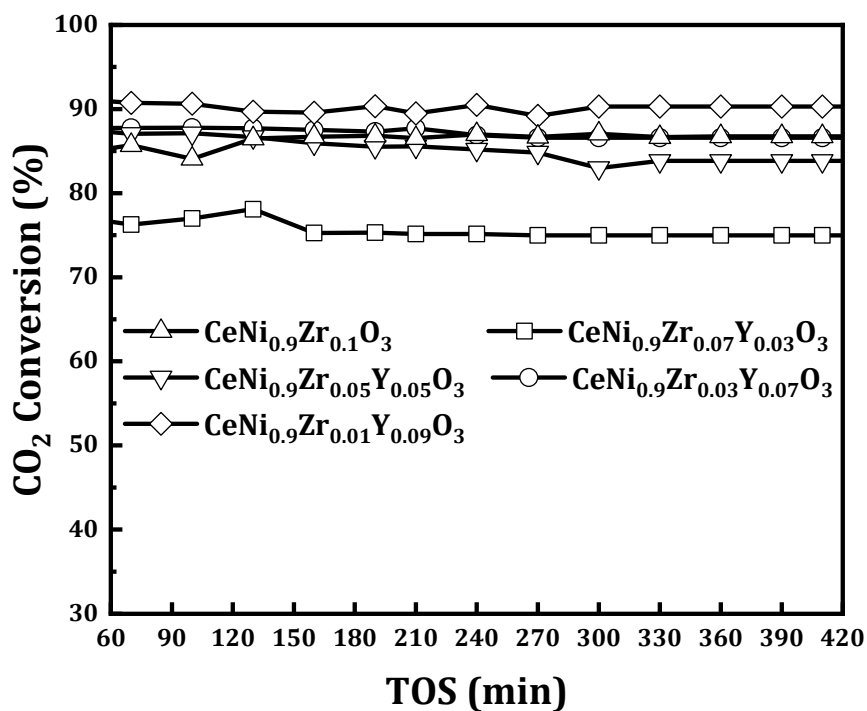

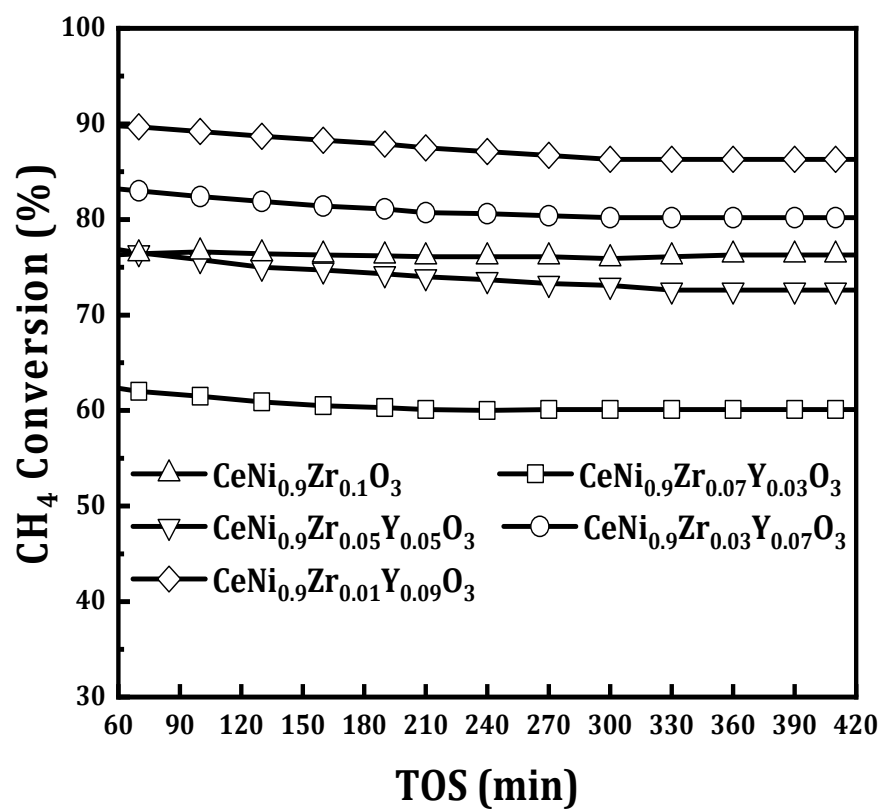**Figure 7.** CO_2 conversion of perovskite catalysts $CeNi_{0.9}Zr_{0.1-x}Y_xO_3$ ($x = 0$, 0.03, 0.05, 0.07, and 0.09) at 800 °C, 1 atmosphere and GHSV = 42 L/(h.g_{cat}).

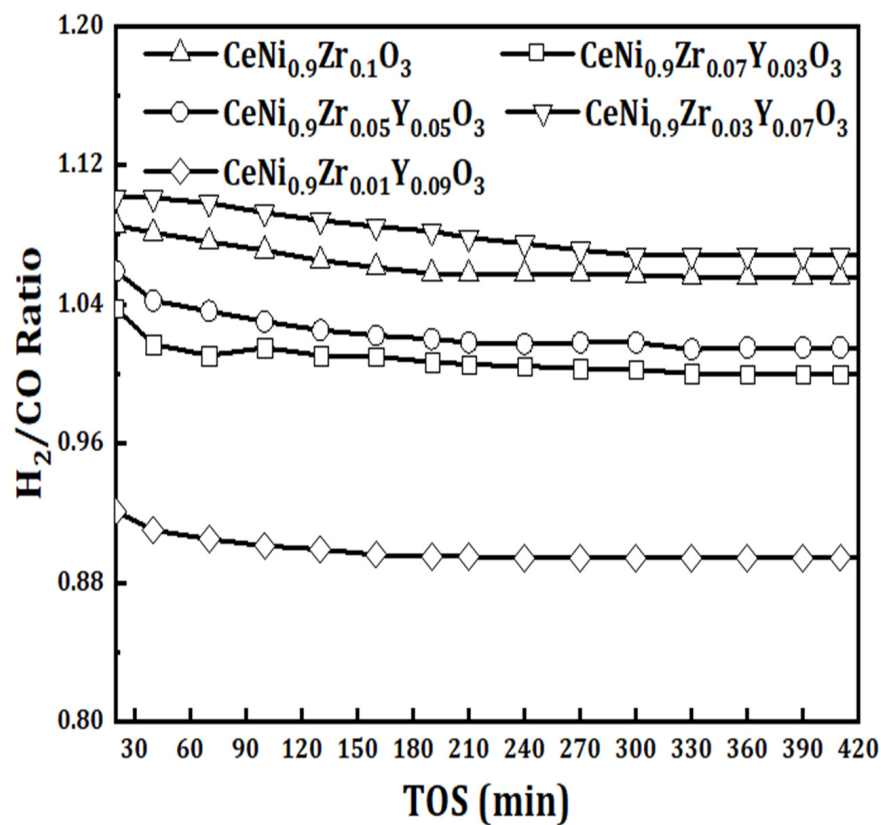**Figure 8.** CH$_4$ conversion of perovskite catalysts CeNi$_{0.9}$Zr$_{0.1-x}$Y$_x$O$_3$ (*x* = 0, 0.03, 0.05, 0.07, and 0.09) at 800 °C, 1 atmosphere and GHSV = 42 L/(h.g$_{cat}$).
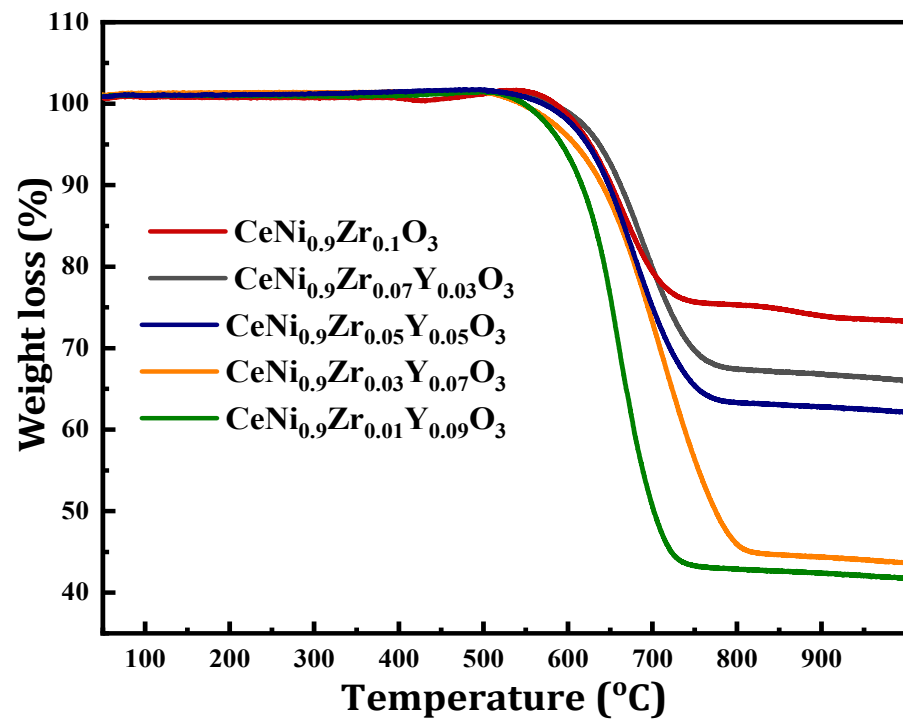

Figure 9. H$_2$/CO ratio of perovskite catalysts CeNi$_{0.9}$Zr$_{0.1-x}$Y$_x$O$_3$ (*x* = 0, 0.03, 0.05, 0.07, and 0.09) at 800 °C, 1 atmosphere and GHSV = 42 L/(h.g$_{cat}$).

Figure 10. TGA Curves of perovskite catalysts $CeNi_{0.9}Zr_{0.1-x}Y_xO_3$ (x = 0, 0.03, 0.05, 0.07, and 0.09) at 800 °C.
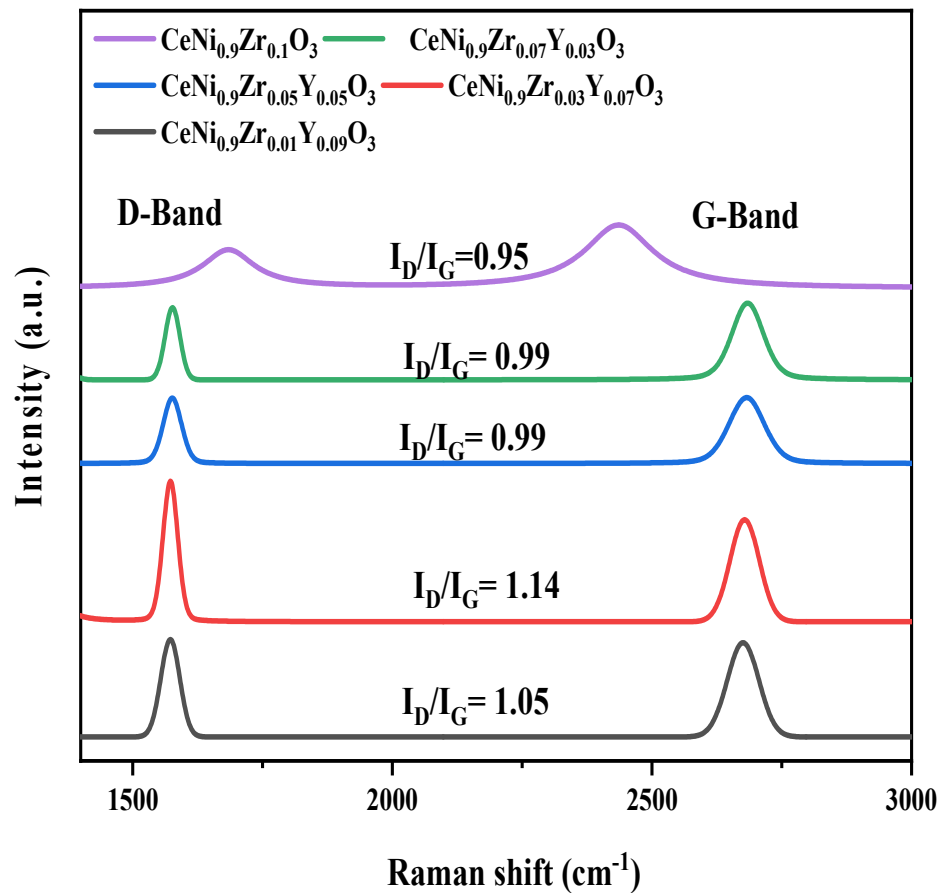

Figure 11. Raman Spectra of Used Perovskite Catalyst $CeNi_{0.9}Zr_{0.1-x}Y_xO_3$ (x = 0.03, 0.05, 0.07, and 0.09).

4. Conclusions

The methane conversion activities of the best-modified catalyst ($CeNi_{0.9}Zr_{0.01}Y_{0.09}O_3$) is significantly higher than the base catalyst ($CeNi_{0.9}Zr_{0.1}O_3$). The amount of the metal ion affects activity as $CeNi_{0.9}Zr_{0.1}O_3$ modified with 0.09Y shows an increase in activity compared to $CeNi_{0.9}Zr_{0.1}O_3$ modified with 0.03Y. The catalyst activity increases with an increase in yttrium loading with $CeNi_{0.9}Zr_{0.01}Y_{0.09}O_3$ catalyst having the best activity with CH_4 conversion >85% and CO_2 conversion >90%. The H_2/CO ratios for $CeNi_{0.9}Zr_{0.1}O_3$ and $CeNi_{0.9}Zr_{0.07}Y_{0.03}O_3$ catalysts are less than one, which suggests that the predominant side reaction is RWGS while $CeNi_{0.9}Zr_{0.05}Y_{0.05}O_3$, $CeNi_{0.9}Zr_{0.03}Y_{0.07}O_3$, and $CeNi_{0.9}Zr_{0.01}Y_{0.09}O_3$ catalysts having H_2/CO ratios greater than one suggests that the Boudouard reaction is the predominant side reaction. The amount of carbon deposited on the catalyst decreases with the increase in zirconium amount hence zirconium helps to improve the catalyst stability being thermally stable.

References

1. Steinhauer, B.; Kasireddy, M.R.; Radnik, J.; Martin, A. Development of Ni-Pd bimetallic catalysts for the utilization of carbon dioxide and methane by dry reforming. *Appl. Catal. A Gen.* **2009**, *366*, 333–341. [CrossRef]
2. Hanley, E.S.; Deane, J.P.; Gallachóir, B.P.Ó. The role of hydrogen in low carbon energy futures—A review of existing perspectives. *Renew. Sustain. Energy Rev.* **2018**, *82*, 3027–3045. [CrossRef]
3. Eilers, J.; Posthuma, S.A.; Sie, S.T. The shell middle distillate synthesis process (SMDS). *Catal. Lett.* **1991**, *7*, 253–269. [CrossRef]
4. Valderrama, G.; Goldwasser, M.R.; de Navarro, C.U.; Tatibouët, J.M.; Barrault, J.; Batiot-Dupeyrat, C.; Martínez, F. Dry reforming of methane over Ni perovskite type oxides. *Catal. Today* **2005**, *107–108*, 785–791. [CrossRef]
5. Ewbank, J.L.; Kovarik, L.; Diallo, F.Z.; Sievers, C. Effect of metal–support interactions in Ni/Al_2O_3 catalysts with low metal loading for methane dry reforming. *Appl. Catal. A Gen.* **2015**, *494*, 57–67. [CrossRef]
6. Oemar, U.; Ang, M.L.; Hidajat, K.; Kawi, S. Enhancing performance of Ni/La_2O_3 catalyst by Sr-modification for steam reforming of toluene as model compound of biomass tar. *RSC Adv.* **2015**, *5*, 17834–17842. [CrossRef]
7. Zou, X.; Wang, X.; Li, L.; Shen, K.; Lu, X.; Ding, W. Development of highly effective supported nickel catalysts for pre-reforming of liquefied petroleum gas under low steam to carbon molar ratios. *Int. J. Hydrogen Energy* **2010**, *35*, 12191–12200. [CrossRef]
8. Shen, K.; Wang, X.; Zou, X.; Wang, X.; Lu, X.; Ding, W. Pre-reforming of liquefied petroleum gas over nickel catalysts sup-ported on magnesium aluminum mixed oxides. *Int. J. Hydrogen Energy* **2011**, *36*, 4908–4916. [CrossRef]
9. Raberg, L.; Jensen, M.; Olsbye, U.; Daniel, C.; Haag, S.; Mirodatos, C.; Sjastad, A. Propane dry reforming to synthesis gas over Ni-based catalysts: Influence of support and operating parameters on catalyst activity and stability. *J. Catal.* **2007**, *249*, 250–260. [CrossRef]
10. Liu, D.; Quek, X.; Cheo, W.N.E.; Lau, R.; Borgna, A.; Yang, Y. MCM-41 supported nickel-based bimetallic catalysts with superior stability during carbon dioxide reforming of methane: Effect of strong metal–support interaction. *J. Catal.* **2009**, *266*, 380–390. [CrossRef]
11. Fakeeha, A.H.; Bagabas, A.A.; Lanre, M.S.; Osman, A.; Kasim, S.O.; Ibrahim, A.A.; Arasheed, R.; Alkhalifa, A.; Elnour, A.Y.; Abasaeed, A.E.; et al. Catalytic Performance of Metal Oxides Promoted Nickel Catalysts Supported on Mesoporous γ-Alumina in Dry Reforming of Methane. *Process* **2020**, *8*, 522. [CrossRef]
12. Lu, H.; Yang, X.; Gao, G.; Wang, J.; Han, C.; Liang, X.; Li, C.; Li, Y.; Zhang, W.; Chen, X. Metal (Fe, Co, Ce or La) doped nickel catalyst supported on ZrO_2 modified mesoporous clays for CO and CO_2 methanation. *Fuel* **2016**, *183*, 335–344. [CrossRef]
13. Zhi, G.; Guo, X.; Wang, Y.; Jin, G.; Guo, X. Effect of La_2O_3 modification on the catalytic performance of Ni/SiC for methanation of carbon dioxide. *Catal. Commun.* **2011**, *16*, 56–59. [CrossRef]

14. De la Cruz, R.G.; Falcón, H.; Peña, M.A.; Fierro, J. Role of bulk and surface structures of $La_{1-x}Sr_xNiO_3$ perovskite-type oxides in methane combustion. *Appl. Catal. B Environ.* **2001**, *33*, 45–55. [CrossRef]

15. De Lima, S.M.; da Silva, A.M.; da Costa, L.O.; Assaf, J.M.; Mattos, L.V.; Sarkari, R.; Venugopal, A.; Noronha, F.B. Hydrogen production through oxidative steam reforming of ethanol over Ni-based catalysts derived from La1−xCexNiO3 perovskite-type oxides. *Appl. Catal. B Environ.* **2012**, *121–122*, 1–9. [CrossRef]

16. Stagg-Williams, S.M.; Noronha, F.B.; Fendley, G.; Resasco, D.E. CO_2 Reforming of CH4 over Pt/ZrO2 Catalysts Promoted with La and Ce Oxides. *J. Catal.* **2000**, *194*, 240–249. [CrossRef]

17. Reddy, G.K.; Loridant, S.; Takahashi, A.; Delichère, P.; Reddy, B.M. Reforming of methane with carbon dioxide over Pt/ZrO2/SiO2 catalysts—Effect of zirconia to silica ratio. *Appl. Catal. A Gen.* **2010**, *389*, 92–100. [CrossRef]

18. Mustu, H.; Yaşyerli, S.; Yasyerli, N.; Dogu, G.; Doğu, T.; Djinović, P.; Pintar, A. Effect of synthesis route of mesoporous zirconia based Ni catalysts on coke minimization in conversion of biogas to synthesis gas. *Int. J. Hydrogen Energy* **2015**, *40*, 3217–3228. [CrossRef]

19. Zhang, X.; Zhang, M.; Zhang, J.; Zhang, Q.; Tsubaki, N.; Tan, Y.; Han, Y. Methane decomposition and carbon deposition over Ni/ZrO2 catalysts: Comparison of amorphous, tetragonal, and monoclinic zirconia phase. *Int. J. Hydrogen Energy* **2019**, *44*, 17887–17899. [CrossRef]

20. Gong, D.; Li, S.; Guo, S.; Tang, H.; Wang, H.; Liu, Y. Lanthanum and cerium co-modified Ni/SiO2 catalyst for CO methanation from syngas. *Appl. Surf. Sci.* **2018**, *434*, 351–364. [CrossRef]

21. Santamaria, L.; Arregi, A.; Alvarez, J.; Artetxe, M.; Amutio, M.; Lopez, G.; Bilbao, J.; Olazar, M. Performance of a Ni/ZrO2 catalyst in the steam reforming of the volatiles derived from biomass pyrolysis. *J. Anal. Appl. Pyrolysis* **2018**, *136*, 222–231. [CrossRef]

22. Damyanova, S.; Shtereva, I.; Pawelec, B.; Mihaylov, L.; Fierro, J.L.G. Characterization of none and yttrium-modified Ni-based catalysts for dry reforming of methane. *Appl. Catal. B Environ.* **2020**, *278*, 119335. [CrossRef]

23. Muñoz, M.; Calvino, J.J.; Rodríguez-Izquierdo, J.; Blanco, G.; Arias, D.; Omil, J.A.P.; Hernandez-Garrido, J.C.; González-Leal, J.; Cauqui, M.; Yeste, M. Highly stable ceria-zirconia-yttria supported Ni catalysts for syngas production by CO_2 reforming of methane. *Appl. Surf. Sci.* **2017**, *426*, 864–873. [CrossRef]

24. Bellido, J.D.A.; Assaf, E.M. Effect of the Y_2O_3–ZrO_2 support composition on nickel catalyst evaluated in dry reforming of methane. *Appl. Catal. A Gen.* **2009**, *352*, 179–187. [CrossRef]

25. Wang, Y.; Li, L.; Wang, Y.; Da Costa, P.; Hu, C. Highly Carbon-Resistant Y Doped NiO–ZrOm Catalysts for Dry Reforming of Methane. *Catalyst* **2019**, *9*, 1055. [CrossRef]

26. Liu, H.R.; Świrk, K.; Galvez, M.E.; da Costa, P. Nickel Supported Modified Ceria Zirconia Lanthanum/Praseodymium/Yttrium Oxides Catalysts for Syngas Production through Dry Methane Reforming. *Mater. Sci. Forum* **2018**, *941*, 2214–2219. [CrossRef]

27. Burbano, M.; Norberg, S.T.; Hull, S.; Eriksson, S.G.; Marrocchelli, D.; Madden, P.A.; Watson, G.W. Oxygen Vacancy Ordering and the Conductivity Maximum in Y_2O_3-Doped CeO_2. *Chem. Mater.* **2011**, *24*, 222–229. [CrossRef]

28. Munteanu, G.; Petrova, P.; Ivanov, I.; Liotta, L.F.; Kaszkur, Z.; Tabakova, T.; Ilieva, L. Temperature-programmed reduction of lightly yttrium-doped Au/CeO2 catalysts: Correlation between oxygen mobility and WGS activity. *J. Therm. Anal.* **2017**, *131*, 145–154. [CrossRef]

29. Fakeeha, A.H.; Kasim, S.O.; Ibrahim, A.A.; Abasaeed, A.E.; Al-Fatesh, A.S. Influence of Nature Support on Methane and CO_2 Conversion in a Dry Reforming Reaction over Nickel-Supported Catalysts. *Materials* **2019**, *12*, 1777. [CrossRef]

30. Verykios, X. Catalytic dry reforming of natural gas for the production of chemicals and hydrogen. *Int. J. Hydrogen Energy* **2003**, *28*, 1045–1063. [CrossRef]

31. Lima, S.; Assaf, J.; Peña, M.; Fierro, J. Structural features of $La_{1-x}Ce_xNiO_3$ mixed oxides and performance for the dry reforming of methane. *Appl. Catal. A Gen.* **2006**, *311*, 94–104. [CrossRef]

32. Pyatnitskii, Y.I.; Bostan, A.I.; Raevskaya, L.N.; Nedil′Ko, S.A.; Dzyaz′Ko, A.G.; Zen′Kovich, E.G. Effect of the Composition of Mn-, Co- and Ni-Containing Perovskites on their Catalytic Properties in the Oxidative Coupling of Methane. *Theor. Exp. Chem.* **2005**, *41*, 117–121. [CrossRef]

33. Peña, M.A.; Fierro, J.L.G. Chemical Structures and Performance of Perovskite Oxides. *Chem. Rev.* **2001**, *101*, 1981–2017. [CrossRef] [PubMed]

34. Ferri, D. Methane combustion on some perovskite-like mixed oxides. *Appl. Catal. B Environ.* **1998**, *16*, 119–126. [CrossRef]

35. Goula, M.A.; Charisiou, N.D.; Siakavelas, G.; Tzounis, L.; Tsiaoussis, I.; Panagiotopoulou, P.; Goula, G.; Yentekakis, I.V. Syn-gas production via the biogas dry reforming reaction over Ni supported on zirconia modified with CeO_2 or La_2O_3 catalysts. *Int. J. Hydrogen Energy* **2017**, *42*, 13724–13740. [CrossRef]

36. Charisiou, N.; Siakavelas, G.; Tzounis, L.; Sebastian, V.; Monzon, A.; Baker, M.; Hinder, S.; Polychronopoulou, K.; Yentekakis, I.; Goula, M. An in depth investigation of deactivation through carbon formation during the biogas dry reforming reaction for Ni supported on modified with CeO_2 and La_2O_3 zirconia catalysts. *Int. J. Hydrogen Energy* **2018**, *43*, 18955–18976. [CrossRef]

37. Świrk, K.; Rønning, M.; Motak, M.; Grzybek, T.; Da Costa, P. Synthesis strategies of Zr- and Y-promoted mixed oxides derived from double-layered hydroxides for syngas production via dry reforming of methane. *Int. J. Hydrogen Energy* **2021**, *46*, 12128–12144. [CrossRef]

38. Fernández, J.M.; Barriga, C.; Ulibarri, M.A.; Labajos, F.M.; Rives, V. New Hydrotalcite-like Compounds Containing Yttrium. *Chem. Mater.* **1997**, *9*, 312–318. [CrossRef]

39. Wang, J.B.; Tai, Y.-L.; Dow, W.-P.; Huang, T.-J. Study of ceria-supported nickel catalyst and effect of yttria doping on carbon dioxide reforming of methane. *Appl. Catal. A Gen.* **2001**, *218*, 69–79. [CrossRef]